Synthesis and crystal structure of RMgSi$_2$ compounds (R = La, Ce, Pr, Nd), a particular example of linear intergrowth

F. Wrubl [a], M. Pani [a,*], P. Manfrinetti [a,b], P. Rogl [c]

[a] *Dipartimento di Chimica e Chimica Industriale, Università di Genova, Via Dodecaneso 31, 16146 Genova, Italy*
[b] *LAMIA Laboratory, CNR-INFM, Corso Perrone 24, 16152 Genova, Italy*
[c] *Institut für Physikalische Chemie, Universität Wien, Währinger Strasse 42, A-1090 Wien, Austria*

ARTICLE INFO

ABSTRACT

A new series of rare earth compounds with stoichiometry RMgSi$_2$ (R = La, Ce, Pr, Nd) is reported. The single crystal X-ray diffraction showed that CeMgSi$_2$, which melts congruently at 1200 °C, crystallizes in a new tetragonal structure type ($I4_1/amd$, $tI32$, $a = 4.2652(4)$ Å, $c = 36.830(4)$ Å, $Z = 8$; w$R_2 = 0.042$ (19 parameters, 393F_0^2), $R_1 = 0.018$ (297$F_0 > 4\sigma F_0$). The crystal structure of CeMgSi$_2$ can be formally built up by alternating along the z direction four CeMg$_2$Si$_2$-type CeMg$_2$Si$_2$ slabs with four AlB$_2$-type CeSi$_2$ slabs, one after the other. The structural model obtained from a CeMgSi$_2$ single crystal has been confirmed for the La, Pr and Nd homologous compounds by means of Rietveld refinement. The trend of the unit-cell parameters, plotted versus the R^{3+} ionic radius, shows a linear behaviour, which strongly suggests a trivalent state for the Ce atoms. An analysis of the features of this new structure is reported, in comparison with the other known CeMg$_2$Si$_2$/AlB$_2$-type linear intergrowth compounds.

1. Introduction

A large number of known structures can be described as a linear intergrowth of slabs along a crystallographic axis [1]: the compounds formed as an intergrowth of Laves phases and CaCu$_5$-type slabs (e.g., CeNi$_3$, Ce$_2$Ni$_7$, PuNi$_3$, Sm$_5$Co$_{19}$), those from CaCu$_5$- and CeCo$_3$B$_2$-type slabs (e.g., CeCo$_4$B, Ce$_3$Co$_{11}$B$_4$), or also of CeAl$_2$Si$_2$- and AlB$_2$-type slabs (e.g., CeAlSi$_2$ and Ce$_3$Al$_4$Si$_4$ [2]). In the latter example, the intergrown slabs share hexagonal meshes of rare earth atoms at their interface (001 plane), and the c-axis of the AlB$_2$ cell is parallel to the intergrowth direction.

When simple basic structure types are intergrown sharing a square mesh at their interface instead of an hexagonal one (BaAl$_4$, CeMg$_2$Si$_2$, AlB$_2$, W, αPo, Cu, AuCu$_3$ and CaF$_2$), other new structure types are formed. In these cases the AlB$_2$ slabs are arranged so that the c axis is perpendicular to the intergrowth direction, sharing the {100} planes at the interface. Considering for example the combination of slabs of BaAl$_4$ and AlB$_2$, the orthorhombic structure types CeNiSi$_2$, U$_3$Ni$_4$Si$_4$ and Ce$_3$Ni$_2$Si$_8$ can be derived. These phases can all be described as a linear combination of the two aforementioned slabs along one crystallographic direction (usually the longest of the new orthorhombic cell), following the stoichiometric equation: $mRX_4 + nRM_2 = R_{m+n}M_{2n}X_{4m}$, so that for CeNiSi$_2$ $m = n = 1$, for U$_3$Ni$_4$Si$_4$ $m = 1$ and $n = 2$ and for Ce$_3$Ni$_2$Si$_8$ $m = 2$ and $n = 1$ [3]. This formal approach has proved to be useful

in the analysis of the structural relationships between members of the same series.

Few literature data exist on the R–Mg–Si phases (R = rare earths) [4–6]. In particular, while the R_2MgSi$_2$ compounds occur for the whole series of rare earths (Mo$_2$FeB$_2$ type, commonly viewed as an intergrowth of CsCl and AlB$_2$ related slabs) [6], the 1:1:1 phase only occurs with the divalent Eu and Yb metals, and CeMg$_2$Si$_2$ (its own type) has been reported only for cerium. As a consequence of our interest on the physical properties of compounds in the Ce–Mg–Si system [5], we synthesized a new phase with stoichiometry CeMgSi$_2$.

In this contribution on the RMgSi$_2$ family of compounds we report about the synthesis and the structural characterization from single crystal (R = Ce) and powder data (R = La, Ce, Pr, Nd). All the phases crystallize in a new tetragonal structure type formed as a linear intergrowth of slabs deriving from the known CeMg$_2$Si$_2$ (CeMg$_2$Si$_2$-type) and CeSi$_2$ (α-ThSi$_2$-type) structures. Structural and chemical features are analyzed in comparison with the other known CeMg$_2$Si$_2$/AlB$_2$-type intergrowth compounds.

The measurements of the physical properties of all the four homologues have just been undertaken and will be part of a future report.

2. Experimental

The elements used were commercial products: 99.9 wt.% for the rare earth elements, 99.98 wt.% for Mg, 'electronic-grade' type (99.9999 wt.% purity) for Si. Samples with nominal composition

"$RMgSi_2$" were prepared for La, Ce, Pr, Nd, Sm and Gd by melting in a high frequency induction furnace (twice, up to 1500 °C) stoichiometric amounts of the elements, sealed by arc welding into outgassed tantalum crucibles in a pure Ar atmosphere. First syntheses were attempted for Ce and Pr, confirming the presence of the 1:1:2 new phase in the as-cast alloys, in a nearly single phase form. A second series of samples was prepared for all the above mentioned R elements. After melting, the crucibles were sealed under vacuum in silica ampoules and then annealed at 1000 °C for 4 days. The so obtained alloys were brittle and small grain sized, showed metallic lustre and were stable toward air and moisture (no changes were visible after a 6 months air exposure).

Metallographic specimens were prepared by standard techniques and examined by both optical (LOM) and electron microscopy (SEM); the 1:1:2 stoichiometry was confirmed by means of microprobe analyses (EDX) for La, Ce, Pr, Nd. A differential thermal analysis (DTA), cycled up to 1300 °C (20 °C/min on heating; 10 °C/min on cooling; ±5 °C accuracy) was performed on an as-cast $CeMgSi_2$ specimen, sealed by arc-welding in a Mo crucible: the results showed that this compound crystallizes congruently at 1200 °C (showing the presence of just one strong thermal effect, detected both on heating and on cooling). After the DTA

cycle, X-ray powder diffraction revealed the presence of the 1:1:2 phase only, as in the other as-cast samples.

X-ray diffraction was carried out both on single crystals and powders. The single crystal analysis was performed for $CeMgSi_2$, selecting a suitable crystal from the DTA sample after a subsequent annealing at 900 °C for 4 days. The intensity data were measured at room temperature by means of a Bruker–Nonius MACH3 diffractometer (graphite-monochromated $MoK\alpha$ radiation, $\lambda = 0.7107 \text{Å}$, point detector). The structure solution was accomplished by means of Patterson methods with SHELXS-97 [7], and the least-squares refinements were carried on with SHELXL-97 [8]; the data collection conditions and the most relevant parameters of the refinement procedure are listed in Table 1. Further details of the crystal structure investigation can be obtained from the Fachinformationszentrum Karlsruhe, 76344 Eggenstein-Leopoldshafen, Germany (fax: +49 7247 808 666; e-mail: crysdata@fiz.karlsruhe.de), on quoting the depository number CSD 419887.

X-ray powder diffraction data were collected with a Guinier–Huber image plate CCD system with Ge monochromated $CuK\alpha_1$ ($8° < 2\theta < 100°$, step $\Delta 2\theta = 0.005°$, 18,401 points). Precise lattice parameters were calculated by least-squares fits to the indexed 4θ-values with Ge as internal standard (99.9999+% purity, $a_{Ge} = 5.657906 \text{Å}$). For Rietveld refinements the FULLPROF suite was used [9]. Pseudo-Voigt functions were used to fit the profiles, with peak asymmetry correction (133 reflections). Either manual point selection or a polynomial function with six parameters was used to fit the background.

All the structural images were produced by means of the free open-source programs DRAWxtl [10], GIMP [11] and the OpenOffice suite [12].

Table 1
Crystal data, data collection conditions and refinements results for the single crystal investigation of the $CeMgSi_2$ compound.
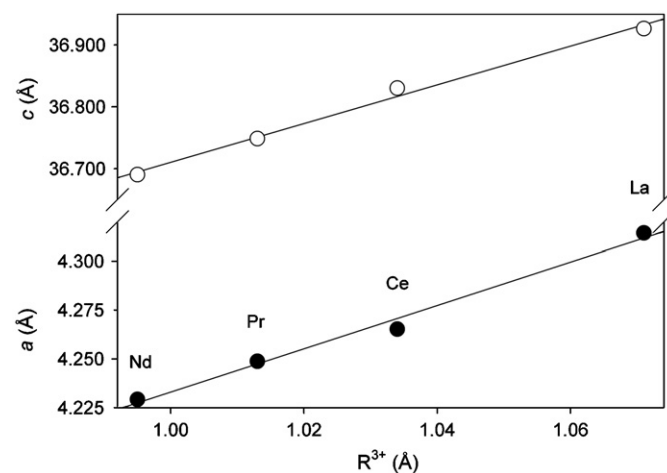
Compound	$CeMgSi_2$
Structure type	$CeMgSi_2$
Crystal system	Tetragonal
Space group	$I4_1/amd$
Lattice parameters (Å)[a]	$a = 4.2652(4)$, $c = 36.830(4)$
Cell volume (Å³)	670.0(2)
Z	8
$F(000)$	784
Formula unit weight (g)	220.596
Pearson code	$tI32$
μ ($MoK\alpha$) (mm^{-1})	14.19
Calculated density (Mg m^{-3})	4.37
Crystal shape	Platelet
Max dimensions (mm)	$0.015 \times 0.13 \times 0.15$
Scan mode	$\omega-\theta$
θ range (°)	2–33
Range in h, k, l	$0 \leqslant h \leqslant 6$, $0 \leqslant k \leqslant 6$, $-56 \leqslant l \leqslant 56$
Measured reflections	1560
Indep. reflections	393
R_{int}	0.044
Refl. with $F_0 > 4\sigma$ (F_0)	297
Transm. ratio (T_{max}/T_{min})	2.59
Absorp. correction	Gaussian integration
Refined parameters	19
Extinction coefficient	0.0017(1)
R_1	0.018
wR_2 (F_0^2) all data	0.042
shift/e.s.d.	0.001
Goodness-of-fit	0.891
$\Delta\rho_{max}$, $\Delta\rho_{min}$ (e Å^{-3})	+0.99, −1.16

[a] From powder data.

Fig. 1. The unit cell parameters of the $RMgSi_2$ compounds (R = La–Nd) plotted vs. the R^{3+} ionic radii.

Table 2
The a and c unit cell parameters, the V_U unit cell volume, the c/a ratio and the $\Delta V\%$ volume contraction for the $RMgSi_2$ compounds.

Compound	Lattice constants (Å)		V_U (Å³)	c/a	ΔV (%)
	a	c			
$LaMgSi_2$	4.3143(4)	36.927(3)	687.3(1)	8.559	14.7
$CeMgSi_2$	4.2652(4)	36.830(4)	670.0(2)	8.635	14.6
$PrMgSi_2$	4.2487(4)	36.749(4)	663.4(2)	8.650	15.2
$NdMgSi_2$	4.2292(5)	36.690(3)	656.2(2)	8.676	15.8

Table 3
Fractional atomic coordinates and anisotropic displacement parameters for $CeMgSi_2$, as obtained from single crystal data.

Atom	z	U_{11} (Å²)	U_{22} (Å²)	U_{33} (Å²)	U_{eq} (Å²)
Ce	0.79775(1)	0.0069(2)	0.0064(2)	0.0051(2)	0.0061(1)
Mg	0.12498(7)	0.0072(10)	0.0137(11)	0.0095(9)	0.0101(4)
Si$_1$	0.26412(5)	0.0098(11)	0.0117(11)	0.0057(7)	0.0091(3)
Si$_2$	0.32695(5)	0.0068(10)	0.0082(10)	0.0058(7)	0.0069(3)

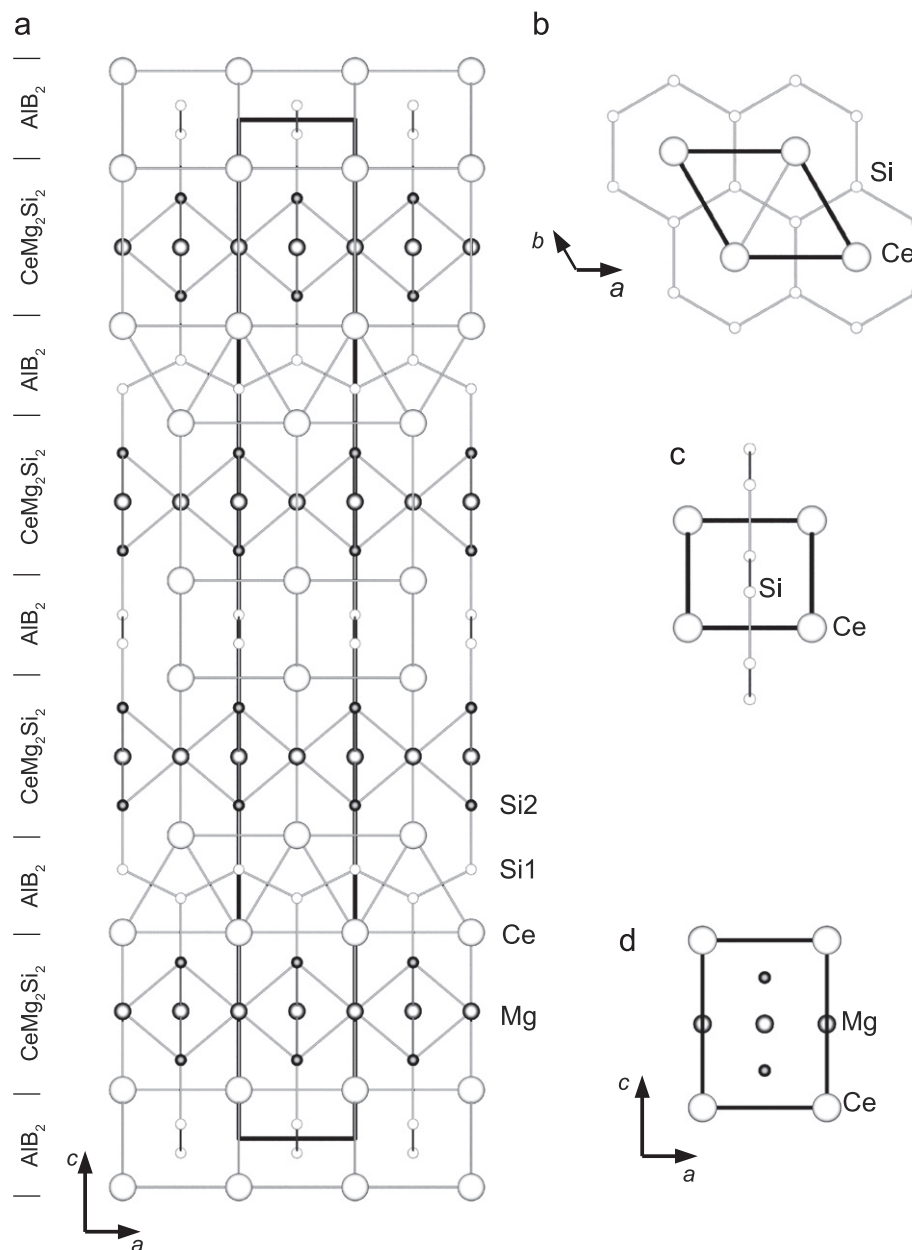All atoms are in (8e): $0, \frac{1}{4}, z$; $U_{12} = U_{13} = U_{23} = 0$.

Fig. 2. The [010] projection of the CeMgSi$_2$ structure: the different slab types are highlighted (a); the CeSi$_2$ (AlB$_2$-type) structure viewed along [001] (b) and [100] (c); the CeMg$_2$Si$_2$ cell along [010] (d).

3. Results

LOM and SEM showed that the RMgSi$_2$ samples were single phase (R = La, Ce), or nearly single phase (R = Pr, Nd), containing traces of Si-rich R–Si binary compounds. The corresponding powder patterns showed immediately that structures isotypic with that of CeMgSi$_2$ were formed by La, Pr and Nd. For Sm and Gd the samples were multiphasic, containing a mixture of RSi$_2$, Mg$_2$Si and R_2MgSi$_2$; no presence of the RMgSi$_2$ phase was observed. After non-plausible results obtained with the TREOR90 program [13], the preliminary single-crystal data on CeMgSi$_2$, i.e. a tetragonal body-centered cell, with a very elongated c-axis, were used for the indexing procedure resulting in a complete interpretation of all powder patterns. The corresponding lattice parameters, together

with the volume contractions[1] observed for these phases, are listed in Table 2. The cell parameters plotted vs. the R^{3+} ionic radius show a linear trend (Fig. 1); the Ce point is aligned, so suggesting a trivalent state for the Ce atoms. It can be observed that, while the unit cell volume V_U regularly decreases from La to Nd (as expected from the lanthanide contraction), the c/a ratio shows a slight increase.

The results of the single crystal analysis (Table 3) show that the CeMgSi$_2$ compound crystallizes in a new ordered structure type.

---

[1] Volume contraction: the relative volume change passing from the separated elements to the intermetallic compound, defined as ΔV (%) = $100(Z\Sigma_i n_i V_i - V_U)/$ $(Z\Sigma_i n_i V_i)$, where Z is the number of formula units in the unit cell, V_i are the atomic volumes and n_i the stoichiometric coefficients; V_U is the observed unit cell volume.

Table 4
Refined positional parameters of the $RMgSi_2$ (R = La, Ce, Pr, Nd) compounds by the Rietveld method.

Compound		R	Mg	Si_1	Si_2	R_B (%)	R_F (%)	R_{WP} (%)	χ^2
LaMgSi$_2$						8.22	5.87	2.63	2.22
	z	0.79800(2)	0.12512(6)	0.26424(6)	0.32725(6)				
	U_{iso} (Å^2)	0.0177(2)	0.0206(8)	0.0216(8)	0.0195(7)				
CeMgSi$_2$						7.67	6.45	3.24	2.71
	z	0.79763(1)	0.12598(6)	0.26405(6)	0.32661(7)				
	U_{iso} (Å^2)	0.0180(2)	0.0288(9)	0.0166(8)	0.0362(9)				
PrMgSi$_2$						8.39	7.27	2.55	6.11
	z	0.79756(2)	0.12546(7)	0.26371(7)	0.32589(8)				
	U_{iso} (Å^2)	0.0203(1)	0.0279(9)	0.0141(9)	0.041(1)				
NdMgSi$_2$						9.33	8.77	3.06	6.98
	z	0.79726(2)	0.12498(8)	0.26459(8)	0.32510(8)				
	U_{iso} (Å^2)	0.0229(3)	0.032(1)	0.022(1)	0.041(1)				

All atoms are in (8e): $0,\frac{1}{4}, z$; R_{WP}: overall agreement index; R_B: Bragg agreement index.
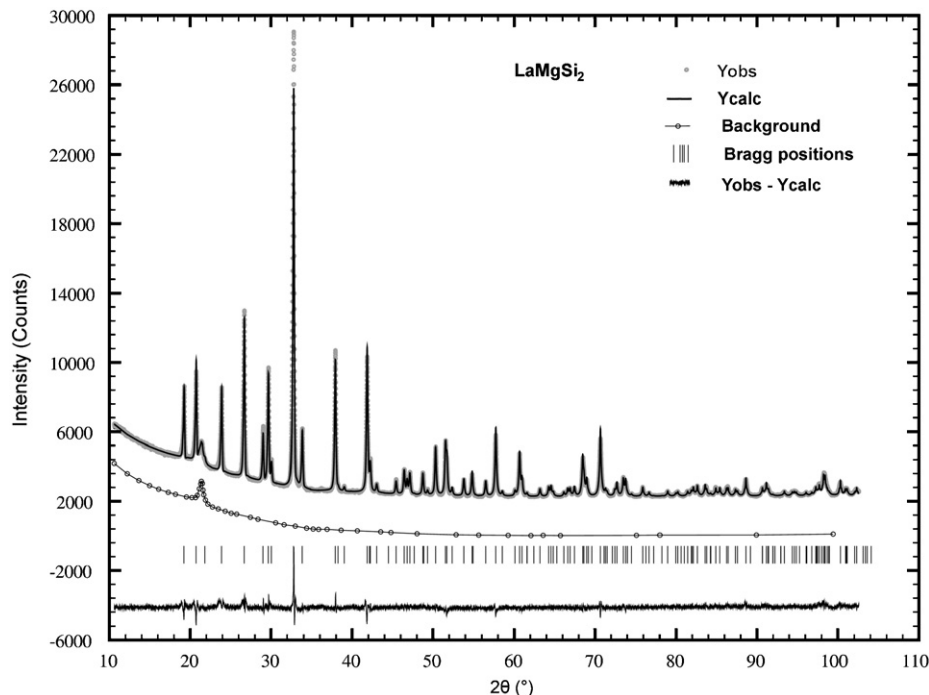
Fig. 3. The observed, calculated and difference X-ray powder diffraction patterns for the LaMgSi$_2$ compound, together with the background points (the visible background peak at $2\theta \cong 21°$ comes from the sample holder foil).

It is a new example of linear intergrowth, resulting from the combination of four AlB$_2$-type CeSi$_2$ slabs and four CeMg$_2$Si$_2$ cells, alternating along the c axis, as shown in Fig. 2. For the sake of comparison, in the same figure the structures of AlB$_2$ (in two projections) and of CeMg$_2$Si$_2$ are shown. Finally, a possible deviation from the fixed 1:1:2 stoichiometry was checked at the end of the anisotropic refinement, allowing the site occupation factors (sof's) of all atoms to freely vary. Only minor deviations of the sof's from unity were obtained (slightly greater than unity for the Ce, Mg and Si$_2$ atoms, and slightly lower than unity (within 4σ) for Si$_1$), correspondingly no significant improvement in the relevant refinement parameters was obtained. Owing to the very small extent of this deviation, in the final cycles all atomic positions were considered fully occupied; however, it is worth

noting that a slight tendency to be defective was shown just by the Si$_1$ atoms, belonging to the AlB$_2$-type slabs; this feature is commonly observed in all known binary phases formed by the rare earths with Si, which always crystallize with defective AlB$_2$ and/or α-ThSi$_2$ structures [4].

Being unavailable any suitable single crystal, for the other members of the series (La, Pr, Nd) the structural model was confirmed by means of Rietveld method and the refined atomic positions are reported in Table 4, along with the isotropic displacement parameters. The agreement indexes R_B, R_F, R_{WP}, as well as the χ^2 values, are also reported in Table 4; the relatively higher χ^2 values obtained for the Pr and Nd samples are ascribable to the presence of few extra unindexed peaks. As an example, the observed, calculated and difference patterns for the LaMgSi$_2$
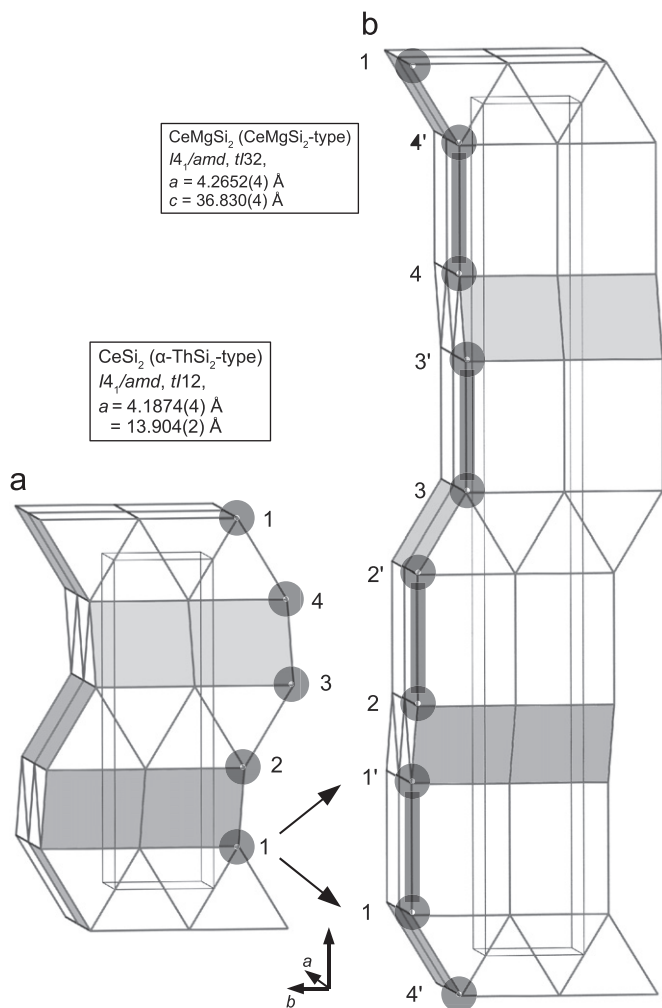
Fig. 4. (a) CeSi$_2$ and (b) CeMgSi$_2$ structures viewed as slab intergrowth along c; the Ce atoms are highlighted and numbered to show the symmetry relationship between the two structures (arrows).

compound are shown in Fig. 3, together with the background points (the visible background peak at $2\theta \cong 21°$ comes from the sample holder foil). For the other samples, the pd_cifs and the corresponding plots are available for download as supplementary material of the present work.

4. Discussion

4.1. Relationship between CeSi$_2$ (α-ThSi$_2$ type) and CeMgSi$_2$

A close relationship holds between CeSi$_2$ (α-ThSi$_2$ type, tI12, I4$_1$/amd) and the new CeMgSi$_2$ compound (Fig. 4a and b). In the unit cell of CeSi$_2$, four AlB$_2$-type CeSi$_2$ slabs are intergrown along the c direction, sharing a square mesh of Ce atoms at the interface at which each next slab is rotated by $\pi/2$ relative to the previous; the presence of the 4$_1$ screw axis along c is thus clear and the complete symmetry is described by the I4$_1$/amd space group. The CeMgSi$_2$ structure has the same overall symmetry; from a symmetry-oriented point of view, the difference is that each plane of cerium atoms forming a CeSi$_2$ slab in the parent α-ThSi$_2$-type structure is now split into two different planes along the c direction, thus leaving enough space to host a whole cell of CeMg$_2$Si$_2$ (CeMg$_2$Si$_2$-type, tP5, P4/mmm). The new CeMgSi$_2$ cell is, therefore, also tetragonal and its symmetry is described by the

Table 5
Interatomic distances for CeMgSi$_2$, as obtained from single crystal data.

|	d (Å)	$d/\Sigma r_{CN12}$
Ce		
2 Si$_1$	3.121(1)	0.99
4 Si$_2$	3.202(1)	1.02
4 Si$_1$	3.260(1)	1.04
2 Mg	3.555(2)	1.13
2 Mg	3.556(2)	1.13
2 Ce	4.114(1)	1.13
4 Ce	4.265(1)	1.17
Mg		
2 Si$_2$	2.771(2)	0.95
2 Si$_2$	2.772(2)	0.95
4 Mg	3.016(1)	0.94
2 Ce	3.555(2)	1.13
2 Ce	3.556(2)	1.13
Si$_1$		
Si$_2$	2.314(3)	0.88
2 Si$_1$	2.373(2)	0.90
2 Ce	3.121(1)	0.99
4 Ce	3.260(1)	1.04
Si$_2$		
Si$_1$	2.314(3)	0.88
2 Mg	2.771(2)	0.95
2 Mg	2.772(2)	0.95
4 Ce	3.202(1)	1.02

same space group of CeSi$_2$, I4$_1$/amd. In the CeSi$_2$ phase the Ce atoms (named as 1, 2, 3, 4 in Fig. 4a) are on the 4a Wyckoff positions, thus lying on the -4 rotoinversion axis $(0,\frac{3}{4},z)$, exactly in correspondence with the inversion centre at $(0,\frac{3}{4},\frac{1}{8})$. In the new structure of CeMgSi$_2$, the Ce atoms are also lying on such a -4 axis, but now they occupy the 8e site at $z = 0.2022$ [$(0,\frac{3}{4},0.2022)$; standard description $(0,\frac{1}{4},0.7978)$], so that—owing to the action of the inversion center—a pair of Ce atoms, symmetrically displaced with respect to $z = \frac{1}{8}$, is generated (atoms 1 and 1' in Fig. 4b). The distance between these two Ce atoms corresponds to the height of all the CeMg$_2$Si$_2$ slabs, and its value of 5.687 Å is only slightly shorter than the c parameter of the CeMg$_2$Si$_2$ phase ($c = 5.765$ Å).

The comparison of the a parameter of CeMgSi$_2$ with those of CeMg$_2$Si$_2$ and of CeSi$_2$ (4.2652(4), 4.250 and 4.1874(4) Å, respectively) shows that in the formation of the CeMgSi$_2$ intergrowth compound the CeSi$_2$ slabs slightly expand, in order to share the square mesh at the interface with the CeMg$_2$Si$_2$ slabs, and not vice-versa.

4.2. Coordination polyhedra

In the new cell each Ce atom (in the 8e position) has coordination number CN = 20; the distances list is reported in Table 5. The coordination polyhedron (Fig. 5a and b), following a modified version of the maximum gap rule [14] (considering the $d/\Sigma r_{CN12}$ maximum gap instead of the d/d_{min} [15]) is coded[2] as $6^{4,2}6^{1,2}4^{6,0}4^{3,1}$ and can be described as formed by a half of the CeMg$_2$Si$_2$-type Ce polyhedron (position 1a, P4/mmm, point symmetry 4/mmm, polyhedron code = $8^{4,1}8^{3,1}4^{4,2}$ [14]; Fig. 5d) and by a half of the α-ThSi$_2$-type Ce polyhedron (position 4a, I4$_1$/amd, point symmetry $-4m2$, polyhedron code $12^{1,2}4^{4,2}4^{2,4}$

---

[2] A series of numbers of coordinating atoms (vertices). The superscripts indicate the number of triangles, squares, pentagons that share each vertex [14].
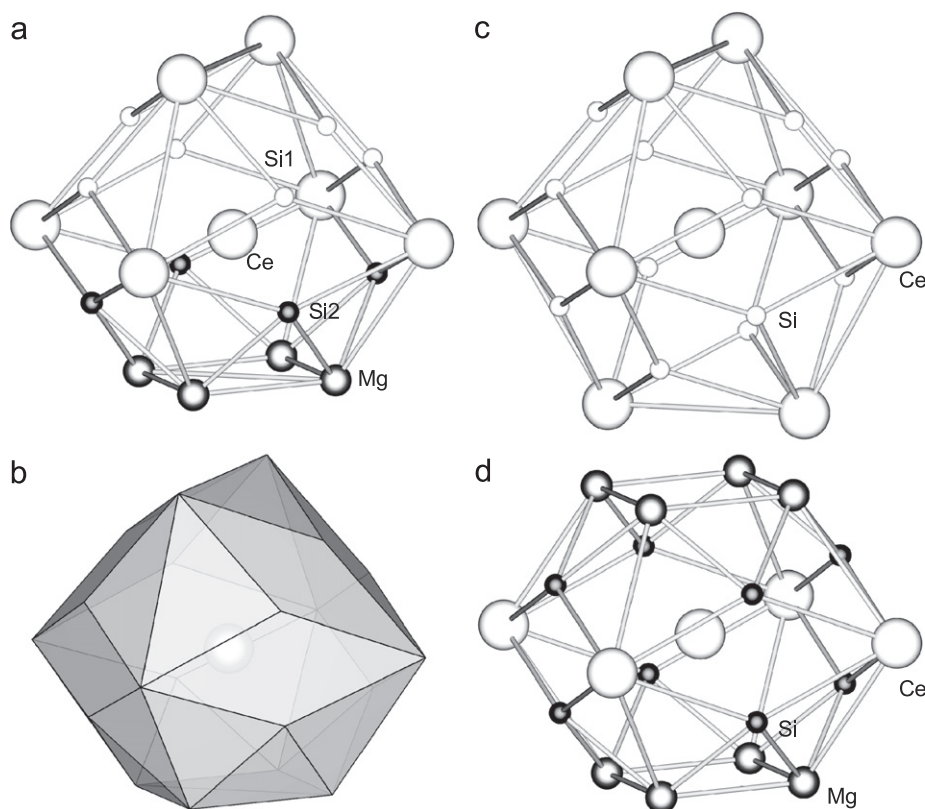
Fig. 5. (a) The Ce coordination polyhedron in $CeMgSi_2$ and (b) the same polyhedron as a solid figure; (c) the Ce coordination polyhedron in $CeSi_2$; (d) the Ce coordination polyhedron in $CeMg_2Si_2$.

[14]; Fig. 5c). This clearly happens because each Ce atom is shared by two slabs of different type. The upper part of the polyhedron, coming from the $CeSi_2$ environment, contributes with $6^{1,2}$ (Si_1) and $2^{4,2}$ (Ce) vertices, while the lower part, coming from the $CeMg_2Si_2$ structure, contributes with $4^{3,1}$ (Si_2), $4^{4,2}$ (Ce) and $4^{6,0}$ (Mg) atoms. The point symmetry reduction from $4/mmm$ to $2mm$, observed at the Ce site passing from $CeMg_2Si_2$ to $CeMgSi_2$, causes the Mg atoms to share six triangles and not four triangles and a square as before. Two Ce–Si_1 distances (3.121 Å) are shorter and four longer (3.260 Å) than those observed in $CeSi_2$ (3.137 and 3.173 Å, calculated from [16], mean distance 3.161 Å), so that the mean distance is now only slightly longer (3.214 Å) in $CeMgSi_2$. On the other side, the Ce–Si_2 distances (3.202 Å) are shorter than the analogous Ce–Si distances in $CeMg_2Si_2$ (3.269 Å).

The Mg atoms retain the same CN = 12 and the polyhedron code $4^{4,1}4^{3,1}4^{2,2}$ as found in $CeMg_2Si_2$, but the point symmetry changed, passing from the parent $CeMg_2Si_2$ structure ($P4/mmm$, position $2e$, point symmetry $mmm.$) to $CeMgSi_2$ ($I4_1/amd$, position $8e$, point symmetry $2mm.$). The loss of the mirror plane perpendicular to c is strictly related to the fact that the four coordinating Mg atoms are no longer lying on a plane with the central Mg and only a two-fold axis is present in the [001] direction (Fig. 6a). Only the Mg–Si_2 distances (2.771 and 2.772 Å) are longer than those observed in the parent structure (2.658 Å), suggesting that the Si_2 atoms are pulled by the bond with the Si_1 atoms in the AlB_2-type slabs.

This bond is also affecting both the Si1 and Si2 coordination polyhedra. The Si1 atoms (CN = 9; Fig. 6b) have the same polyhedron code $6^{5,0}3^{4,0}$ and the same $2mm.$ point symmetry as Si in the α-$ThSi_2$-type $CeSi_2$. In both structures the bonds between Si atoms belonging to different slabs (Si_1–Si_2 in $CeMgSi_2$) are

shorter than those between the atoms belonging to the same slab (Si_1–Si_1 in $CeMgSi_2$); in $CeMgSi_2$, this phenomenon is slightly attenuated because the bonds Si_1–Si_1 = 2.373 Å are already relatively shorter than in $CeSi_2$ (intraslab Si–Si = 2.411 Å; interslab Si–Si = 2.280; Si_1–Si_2 = 2.314 Å, comparable to twice as the Si covalent radius r_{cov} = 1.17 Å). This short Si_1–Si_2 bond is part of a truncated three-dimensional Si network (Fig. 2a), centered in every AlB_2-type slab, that is clearly related to the three-dimensional network found in $CeSi_2$ [17]. The presence of this shorter Si_1–Si_2 bond is, as expected, also reflected in the Si2 coordination polyhedron, CN = 9. It has the shape of a slightly distorted mono-capped square antiprism, coded as $4^{5,0}2^{5,0}2^{4,0}1^{4,0}$ (Fig. 6c), different from that observed in $CeMg_2Si_2$ (CN = 10, bicapped square antiprism, polyhedron code $8^{5,0}2^{4,0}$). Also in this case the change of the space group and Wyckoff position of the atoms (from $2h$, $P4/mmm$, point symmetry $4mm$, to $8e$, $I4_1/amd$, point symmetry $2mm.$) causes a point symmetry reduction, so that the polyhedron still has the {100} mirrors, but it has lost the {110} mirrors and the fourfold axis along c. This is once again related to the coplanarity loss of the Mg atoms. Besides the point symmetry, the main difference is related to the two Si–Si bond distances, one being remarkably shorter (Si_2–Si_1, 2.314 Å) and the other longer (Si_2–Si_2, 3.536 Å) than the corresponding ones found in $CeMg_2Si_2$ (2.571 and 3.194 Å, respectively). The two Si2 atoms inside the $CeMg_2Si_2$-type slabs are thus symmetrically moving apart, along c, from the pseudo-square of the four Mg atoms, each one pulled by the covalent bond with one of the two symmetrical Si1 atoms in the surrounding AlB_2-type slabs. Since the $CeMg_2Si_2$ slabs undergo in the same time a very small contraction along c as already mentioned (from 5.765 to 5.687 Å), this implies that the Si2–Ce distance is also contracted, from 3.269 to 3.202 Å.
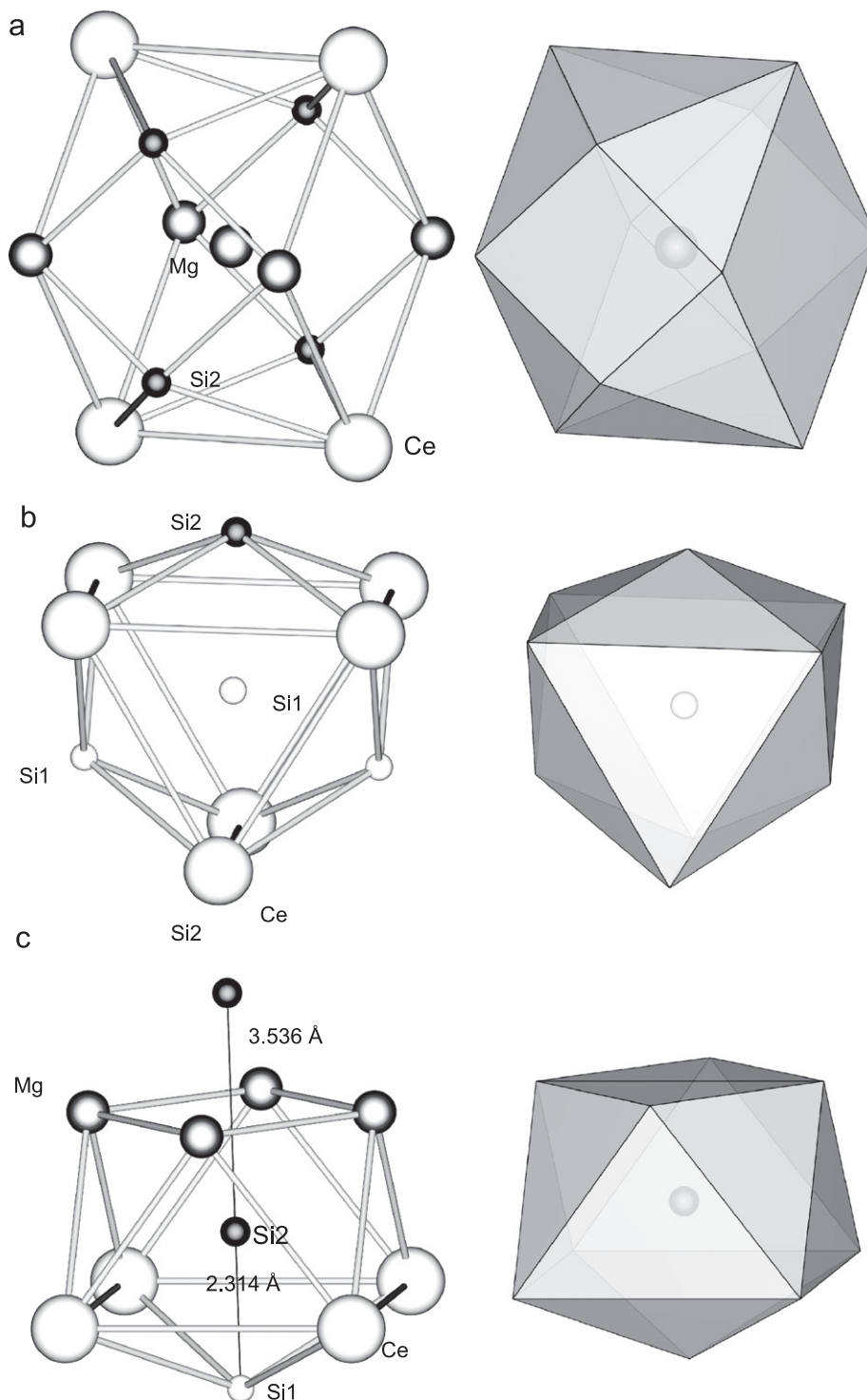
Fig. 6. The coordination polyhedra of (a) Mg, (b) Si1 and (c) Si2, in CeMgSi$_2$, as bond connections and as solid figures.

3.4. Comparison with other CeMg$_2$Si$_2$/AlB$_2$ linear intergrowth structures

The RMgSi$_2$ compounds are part of the general series $R_{m+n}M_{2m}X_{2(m+n)}$ (formally formed by mRM_2X_2 and nRX_2, with $m = 1$, $n = 1$; Fig. 7a). In the R–M–X ternary systems (R = rare earth, M = transition element, Li or Mg, X = p-element) the only other known member of this series is represented by NdNiGa$_2$, oC16, with again $m = n = 1$, formed by two CeMg$_2$Si$_2$-type

NdNi$_2$Ga$_2$ slabs[3] and two AlB$_2$-type NdGa$_2$ slabs, alternating along the NdNiGa$_2$ b direction ([18]; Table 6; Fig. 7b; the same structure is adopted by all the RNiGa$_2$ compounds (R = La–Gd) [19]). No other compound belonging to this system is known with different

---

[3] The Ga atoms replace the Mg atoms and the Ni the Si ones in the CeMg$_2$Si$_2$-type slabs, and this change does not affect the overall 1:1:2 stoichiometry of the intergrowth phase.
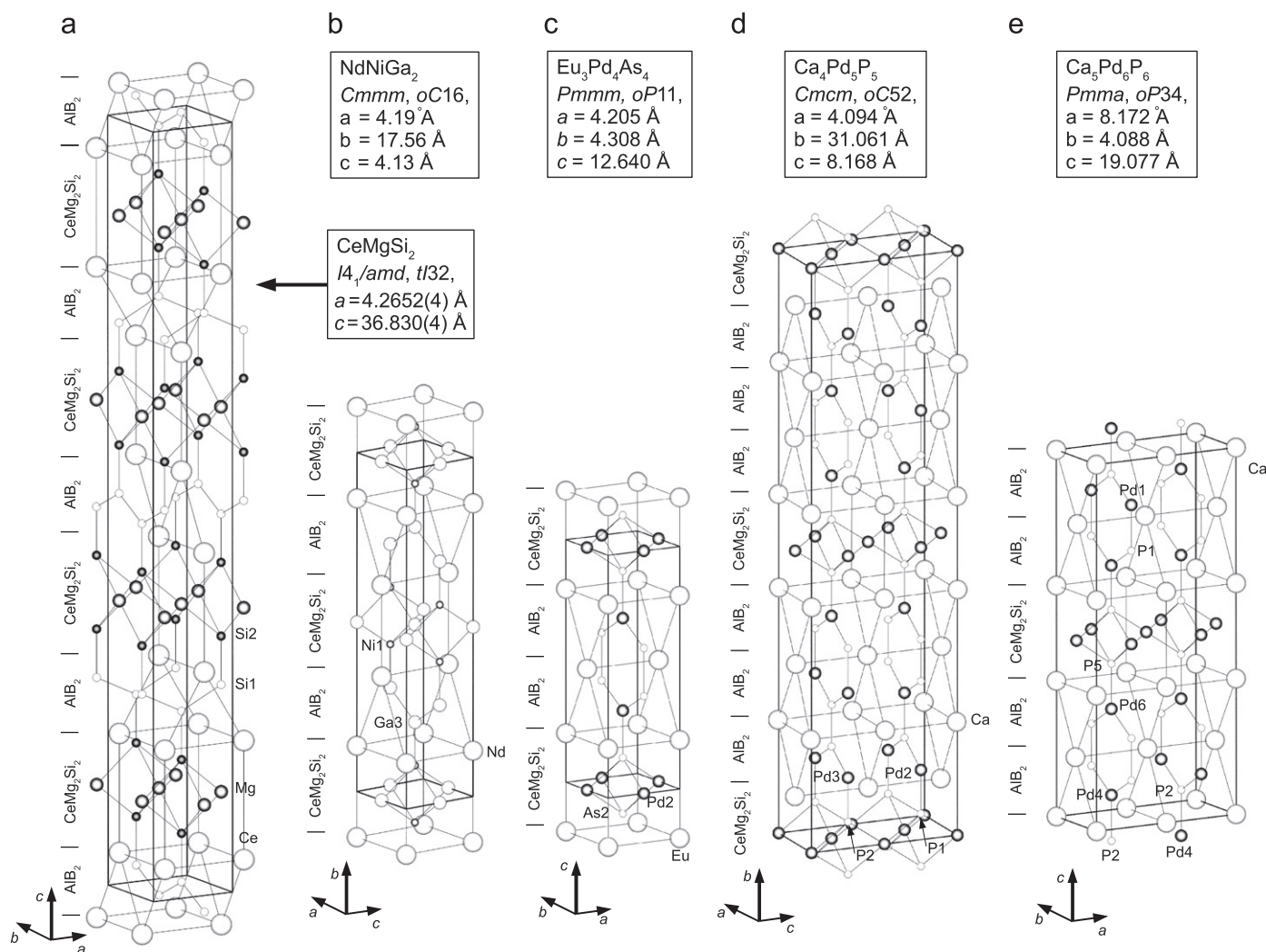
Fig. 7. Comparison of CeMg$_2$Si$_2$ with the other known CeMg$_2$Si$_2$/AlB$_2$-type intergrowth structures; the different slab types are highlighted.

Table 6
The series of the known CeMg$_2$Si$_2$/AlB$_2$ intergrowth compounds: formula, m and n parameters, Pearson code.

Formula	m (CeMg$_2$Si$_2$-type)	n (AlB$_2$-type)	Pearson symbol	Ref.
CeMgSi$_2$	1 (CeMg$_2$Si$_2$)	1 (CeSi$_2$)	tI32	This work
NdNiGa$_2$	1 (NdNi$_2$Ga$_2$)	1 (NdGa$_2$)	oC16	[13]
Eu$_3$Pd$_4$As$_4$	1 (EuPd$_2$As$_2$)	2 (EuPdAs)	oP11	[19]
Ca$_4$Pd$_5$P$_5$	1 (CaPd$_2$P$_2$)	3 (CaPdP)	oC56	[19]
Ca$_5$Pd$_6$P$_6$	1 (CaPd$_2$P$_2$)	4 (CaPdP)	oP34	[19]
CeSi$_2$ (α-ThSi$_2$)	0	4 (CeSi$_2$)	tI12	[13,16]
CeMg$_2$Si$_2$	1	0	tP5	[13]

m:n ratio. It can be underlined that, in these two cases of intergrowth structures, the two slab types are present within the unit cell in different overall numbers (4 and 2) but have the same relative weight ($m = n = 1$). Few other CeMg$_2$Si$_2$/AlB$_2$ intergrowth compounds are known. They are shown in Fig. 7c–e. Johrend and Mewis [20] reported about two alkaline-earth palladium phosphides and one europium palladium arsenide, crystallizing with their own structure types. All these three structures are members of the general series $A_{m+n}Pd_{2m+n}X_{2m+n}$ (A = alkaline-earth or europium, X = arsenic or phosphorous), in which m is again the number of fragments with composition APd_2X_2 (CeMg$_2$Si$_2$-type) and n is the number of fragments with composition $APdX$ (SrPtSb-type, ternary variant of the AlB$_2$-type). For each compound m and n are given in Table 6. As an example, for Ca$_4$Pd$_5$P$_5$ $m = 1$ and $n = 3$; it is formed by the linear intergrowth of two slabs of CaPd$_2$P$_2$ and six of CaPdP (Fig. 7d). In a ternary A–Pd–X diagram, all the compounds belonging to the series reported by Mewis lie on the straight line of the pseudo-binary system formed by the 1:2:2 and the 1:1:1 ternary compounds. The intermediate intergrowth compounds, found between the 1:2:2 and the 1:1:1 phases, can be regarded as a step-by-step "dilution" of the 1:2:2 phase with A, since the ratio Pd:X = 1 remains constant along the line and the A content increases stepwise from 20 up to 33 atomic %.

From a detailed geometric analysis, the five structures can be divided into three groups: (i) pure tetragonal structures (CeMgSi$_2$ as well as CeSi$_2$), (ii) structures with orthorhombic distortions (NdNiGa$_2$ and Eu$_3$Pd$_4$As$_4$) and (iii) true orthorhombic structures (Ca$_4$Pd$_5$P$_5$ and Ca$_5$Pd$_6$P$_6$). The AlB$_2$ slabs always have their c direction (connecting the triangular bases of the trigonal prisms) perpendicular to the intergrowth direction. If, within one unit cell of the derived structure, the c and a directions of the intergrown AlB$_2$ slabs are regularly interchanged, being either perpendicular or antiparallel, the two parameters are forced to find a unique

compromise value, and a tetragonal cell is thus adopted. If instead they always lie on the same direction, these become distinguishable and, as a result, an orthorhombic distortion is obtained.

4.5. Inter/intra slab interactions

For comparison, it can be useful to consider how the coordination polyhedra change from the parent structures to the intergrown slabs in the new compounds, and also for other kinds of linear intergrowth series.

In the case of the abovementioned $CeAlSi_2$, $CeAl_2Si_2/AlB_2$ intergrowth compound ($m:n = 1$, with an hexagonal mesh at the interface) only the Ce atom is coordinated by atoms belonging to slabs of both types [2]. The other atoms are coordinated only by vertices belonging to the same slab: the interaction between slabs of different type can thus be supposed to be not very different to that between slabs of the same type. This means that other intergrowth structures with contiguous $CeAl_2Si_2$-type slabs should be considered as equally stable, and in fact the $Ce_3Al_4Si_6$ structure type ($m = 2$, $n = 1$, $m:n = 2$) is also observed [2].

On the other hand, in $CeMg_2Si_2$ and in all the other known $CeMg_2Si_2/AlB_2$ intergrowth structures, strong bonding interactions between slabs of different type can be noticed, as resulting from the covalent bonds between atoms belonging to slabs of different type. These bonds are absent in the interaction between slabs of the same type in the bulk $CeMg_2Si_2$ phase. As for $CeMgSi_2$, this phenomenon is clearly reflected on the coordination polyhedra of the $NdNiGa_2$ structure [14]; the Nd atoms are surrounded, as expected, by atoms of both the slabs; also the Ni and the Ga3 atoms are involved in inter-slab bonds, because a strong Ni–Ga bond is formed ($d_{Ni-Ga3} = 2.248$ Å, shorter than the 2.41 Å sum of the covalent radii; Fig. 7b). This is indeed the analogue of the Si1–Si2 bond in the $CeMgSi_2$ structure. Analogous strong interactions are found in $Eu_3Pd_4As_4$ between the Pd2 and As2 atoms ($d_{Pd2-As2} = 2.458$ Å [20], whereas the sum of the covalent radii is 2.48 Å), in $Ca_4Pd_5P_5$ between the couples Pd2–P1 and Pd3–P2 ($d_{Pd2-P1} = 2.323$ Å, $d_{Pd3-P2} = 2.342$ Å, whereas the sum of the covalent radii is 2.34 Å) and in $Ca_5Pd_6P_6$ between the pairs Pd2–P4 and Pd6–P5 ($d_{Pd2-P4} = 2.310$ Å, $d_{Pd6-P5} = 2.365$ Å), as shown in Fig. 7b–d). If two $CeMg_2Si_2$-type slabs were connected, only one short Si–Si bond per unit cell out of two possible would form, and the structure would be thus less favoured. As a direct consequence, are only formed intergrowth structures where the $CeMg_2Si_2$-type slabs are strictly intergrown between AlB_2-type slabs, meaning that this kind of sequence is more stable than that/those with contiguous $CeMg_2Si_2$-type slabs. To the best of our knowledge, structures of this type have not yet been found.

On the other hand, the intergrowth of consecutive AlB_2 slabs is for these phases also accompanied by the formation of directional covalent bonds, that can be either hetero-atomic (in $Ca_5Pd_6P_6$ $d_{Pd1-P1} = 2.386$ Å, in $Ca_4Pd_5P_5$ $d_{Pd5-P4} = 2.389$ Å) or homo-atomic (in $Eu_3Pd_4As_4$ $d_{As1-As1} = 2.505$ Å). All the above-mentioned intergrowth compounds are thus formed with $m = 1$ and $n = 1, 2, 3$ or 4 (Table 6).

In the Ce–Mg–Si system, the intergrowth of consecutive AlB_2-type $CeSi_2$ slabs would lead to the formation of Si–Si bonds, like it happens in the α-$ThSi_2$ structure, where a three-dimensional network of silicon atoms is formed. The existence of other members of the $R_{m+n}M_{2m}X_{2m+n}$ series, with $m:n > 1$ can thus not be excluded *a priori*. This chance is currently under investigation and will be reported in due time.

Acknowledgment

References

[1] E. Parthé, B. Chabot, in: K. Gschneidner, L. Eyring (Eds.), Handbook on the Physics and Chemistry of Rare Earths, vol. 6, Elsevier Science, Amsterdam, 1984, p. 113.
[2] H. Flandorfer, P. Rogl, J. Solid State Chem. 127 (1996) 308.
[3] Y. Yarmolyuk, L. Aksel'rud, Y. Grin', V. Fundamenskii, E. Gladyshevskii, Sov. Phys. Crystallogr. 24 (1979) 332.
[4] CRYSTMET—The Metals Database, V.3.7.0, Tooth Information System Inc., 2008.
[5] S.K. Dhar, P. Manfrinetti, A. Palenzona, J. Alloys Compd. 252 (1997) 24.
[6] R. Kraft, R. Pöttgen, Monatsh. für Chem. 136 (2005) 1707.
[7] G.M. Sheldrick, SHELXS-97, Program for Crystal Structure Solution, University of Göttingen, Germany, 1997.
[8] G.M. Sheldrick, SHELXL-97, Program for Refinement of Crystal Structures, University of Göttingen, Germany, 1997.
[9] J. Rodriguez-Carvajal, Physica B 192 (1993) 55.
[10] L.W. Finger, M. Kroekerb, B.H. Toby, J. Appl. Crystallogr. 40 (2007) 188.
[11] ⟨http://www.gimp.org⟩.
[12] ⟨http://www.openoffice.org⟩.
[13] P. Werner, L. Eriksson, A. Santoro, J. Appl. Crystallogr. 18 (1985) 367.
[14] J.L. Daams, P. Villars, J. van Vucht, Atlas of Crystal Structure Types for Intermetallic Phases, ASM, 1991.
[15] G. Bruzzone, M.L. Fornasini, F. Merlo, J. Less-Common Met. 22 (1970) 252.
[16] A. Morozkin, V. Stupnikov, V. Nikiforov, N. Imaoka, I. Morimoto, J. Alloys Compd. 415 (2006) 12.
[17] W. Zachariasen, Acta Crystallogr. 2 (1949) 94.
[18] E. Parthé, L. Gelato, B. Chabot, M. Penzo, K. Cenzual, E. Gladyshevskii, Gmelin Handbook of Inorganic and Organometallic Chemistry, vol. 1, Springer, Berlin, 1993, p. 145.
[19] Y. Grin', Y. Yarmolyuk, Dopov. Akad. Nauk Ukr. RSR Ser. A 44 (1982) 69.
[20] D. Johrendt, A. Mewis, Z. Anorg. Allg. Chem. 621 (1995) 57.